International Journal of Multiphase Flow 34 (2008) 1142–1151

Contents lists available at ScienceDirect

International Journal of Multiphase Flow

journal homepage: www.elsevier.com/locate/ijmulflow

Turbulent cascade modeling of single and bubbly two-phase turbulent flows

Igor A. Bolotnov *, Richard T. Lahey Jr., Donald A. Drew, Kenneth E. Jansen

Center for Multiphase Research, Rensselaer Polytechnic Institute, 110 8th Street, Troy, NY 12180, USA

ARTICLE INFO

Article history:
Received 7 February 2008
Received in revised form 20 June 2008
Accepted 27 June 2008
Available online 9 July 2008

ABSTRACT

The analysis of turbulent two-phase flows requires closure models in order to perform reliable computational multiphase fluid dynamics (CMFD) analyses. A spectral turbulence cascade-transport model, which tracks the evolution of the turbulent kinetic energy from large to small liquid eddies, has been developed for the analysis of the homogeneous decay of isotropic single and bubbly two-phase turbulence. This model has been validated for the decay of homogeneous, isotropic single and two-phase bubbly flow turbulence for data having a 5 mm mean bubble diameter. The Reynolds number of the data based on bubble diameter and relative velocity is approximately 1400.

1. Introduction

Current generation computer systems do not have enough computational power to perform direct numerical simulations (DNSs) of complex single and two-phase flow systems at high Reynolds numbers. Thus good closure models for Reynolds-averaged Navier–Stokes (RANS) computational multiphase fluid dynamic (CMFD) analyses are still required in engineering analyses. Various closure models have been developed in the past to approximate turbulence phenomena in the RANS conservation equations for single-phase flows (Pope, 2000). The complexity of these models range from the Prandtl mixing length, k–ε and other similar transport models involving one or two transport equations (Wilcox, 2002), to more complex models (Lumley, 1978), where turbulent anisotropy is evaluated. There has been some success in extending k–ε type models to bubbly two-phase flows (Lahey, 2005), but these models are limited to low void fractions.

The spectral cascade model presented in this paper belongs to the class of models called shell models (Bohr et al., 1998). Shell models consider a discrete set of wave vectors, or shells, in Fourier space and solve a set of differential equations using one or two variables per shell. A good overview of various shell models is given by Bohr et al. (1998). Desnyanski and Novikov (1974) proposed the idea of using shells to model the energy cascade process and to be able to reproduce the Kolmogorov spectrum in terms of appropriate differential equations for the averaged velocity field in Fourier space. Ohkitani and Yamada (1989) introduced a shell model (the so-called GOY model) with one complex variable per shell as a generalization of Gledzer (1973) model which had one real variable per shell. The GOY model features interactions between nearest and next nearest neighboring shells and conserves energy as well as volume in phase space.

Schiestel (1987) introduced a multiple-time-scale model which is based on partial integration of the spectral evolution equations in wavelength intervals. Schiestel used the so-called Kovasznay hypothesis (Hinze, 1975) to model the spectral transfer. In the present work, we have also used a Kovasznay transfer term. Chaouat and Schiestel (2005) have also used this spectral transfer concept to propose a new model for large eddy simulation (LES) by tracking the energy transfers for the sub-grid turbulent kinetic energy.

Spectral turbulent kinetic energy information can help us model the energy transfers between liquid eddies of different sizes and the energy exchanges between dispersed bubbles and liquid eddies. Single-phase experiments on the decay of isotropic turbulence (Comte-Bellot and Corrsin, 1966) give the energy spectrum at different distances from the turbulence generating grids. Also, Kang et al. (2003) used an active grid to generate a relatively high Reynolds number isotropic turbulent flow and proposed an analytical expression based on their experimental data for energy spectrum's time dependence for the decay of single-phase turbulence.

Jairazbhoy et al. (1995a,b) used a spectral cascade turbulence model, coupled with a droplet number density transport model, to analyze neutral buoyant droplets immersed in homogeneously turbulent gas, in which breakup and coalescence were modeled. If coalescence and breakup are not considered then the spectral cascade model can be greatly simplified, and this is the approach we have taken.

DNS can also provide insight into the energy transfers and eddy interactions. Domaradzki and Rogallo (1990) and Domaradzki et al. (1994) analyzed the energy spectrum and energy transfers in wave number space using DNS. It was concluded that 75% of the liquid eddy interactions occur in local wave number triads with the ratio of the two legs of the triad being less than 2 (i.e., between neighboring eddy sizes).

Currently there is not universal agreement in the literature on the slope of the energy spectrum for bubbly two-phase flows. Quite

* Corresponding author. Tel.: +1 518 276 8126; fax: +1 518 276 3055.
E-mail address: boloti@rpi.edu (I.A. Bolotnov).

0301-9322/$ - see front matter © 2008 Elsevier Ltd. All rights reserved.
doi:10.1016/j.ijmultiphaseflow.2008.06.006

a few experiments and DNSs report a slope of −5/3, or one "slightly less steep than −5/3" (Rensen et al., 2005), while others have found different slopes. To properly analyze the slopes of the energy spectrum one must be careful to look at the same range and the same system of coordinates when comparing these slopes. Generally, we may have two separate slopes in the energy spectrum; one slope in the inertial subrange and a steeper slope in the dissipation range. For example, Lance and Bataille (1991) report a −5/3 slope for the inertial subrange of turbulent single-phase flow and −8/3 for their corresponding bubbly two-phase flow experiments. However, a careful analysis of their two-phase spectrum (see Fig. 1) shows that Lance and Bataille (1991) actually had a slope between −8/3 and −11/3 in the high wave number dissipation range and a ∼−7/6 slope in the inertial subrange of the corresponding single-phase flow. Since −7/6 is slightly less steep than −5/3, their results are in substantial agreement with the data of Rensen et al. (2005).

Bunner and Tryggvason (2003) performed a 3-D DNS of 27 deformable bubbles rising in a periodic domain. They analyzed the induced turbulent kinetic energy spectrum in the liquid phase and found a −3.6 slope in the dissipation region. This slope is very close to a −11/3 slope (i.e., −3.67) which, as noted above, can also be seen in the data of Lance and Bataille (1991).

2. Discussion

This paper describes a single and two-phase spectral turbulent cascade-transport model which was developed and used for the analysis of the homogeneous decay of isotropic turbulent flows. This spectral model tracks the evolution of turbulent kinetic energy through wave number space. The sum of the cascade model's transport equations for turbulent kinetic energy (k) yields the total turbulent kinetic energy transport equation used in k–ε models (Jones and Launder, 1972). A dispersed phase can influence the turbulent kinetic energy of the continuous liquid phase and models have been developed and used for bubbly two-phase flow calculations by superimposing a bubble-induced turbulence source term in the single-phase k–ε transport equations (Lahey, 2005). However, this non-spectral superposition model is only valid for low void fractions (Lahey, 2005).

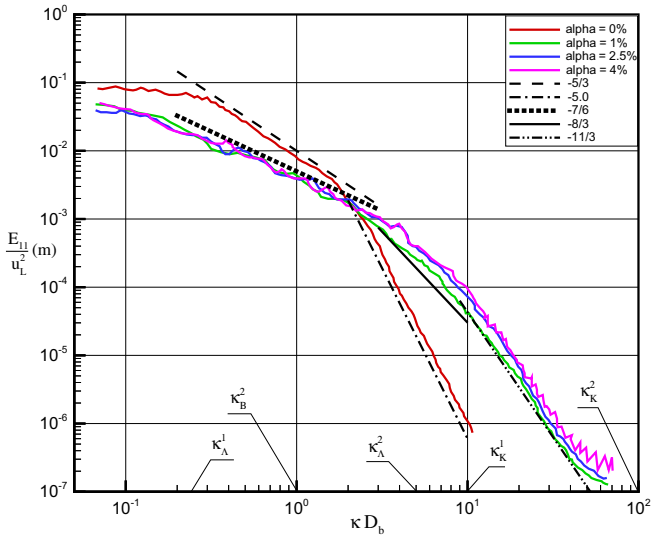

Fig. 1. One-dimensional spectrum of Lance and Bataille (1991). Experiments for different void fractions, α (U_L = 0.9 m/s; X/M = 36.4; D_b = 5 mm). The Taylor ($\kappa_\Lambda^1, \kappa_\Lambda^2$) and Kolmogorov ($\kappa_K^1, \kappa_K^2$) scales shown for both single (1) and two-phase (2) cases; the bubble's scale (κ_B^2) is also shown, for D_b = 5 mm.

The turbulent cascade model presented herein is based on a spectral representation of the turbulent kinetic energy of the continuous liquid phase, and it follows the work of Lewalle and Tavlarides (1994). The energy is split into spectral bins and each bin contains the turbulent kinetic energy for liquid eddies of specific sizes. The model considers a net turbulent cascade of the kinetic energy from the largest liquid eddies of the flow to the smallest ones. Significantly, knowledge of the spectral distribution of the turbulent kinetic energy allows one to eliminate the empirical turbulent dissipation rate transport equation, using an explicit expression instead.

3. The cascade model

In a spectral turbulent cascade model the energy of the turbulent liquid eddies of each characteristic group size is represented with a separate variable. As shown schematically in Fig. 2, the whole spectrum of eddy sizes is covered with these discrete energy bins. Thus, at any given point the sum of the spectral energies equals the total turbulent kinetic energy of the continuous liquid phase:

$$k = \sum_{m=1}^{N} k_m \tag{1}$$

where N is total number of spectral bins.

Since we have to cover the whole energy spectrum, we must estimate the largest and the smallest eddy sizes for a given problem. The smallest eddy size of interest corresponds to the Kolmogorov scale ($\lambda_N \equiv \eta = 2\pi/\kappa_N$, where $\eta = \nu^{3/4}/\varepsilon^{1/4}$) while the largest scale depends upon the geometry of the problem ($\lambda_0 = 2\pi/\kappa_0$). If the number of bins is insufficient in the dissipation region then we will observe an accumulation of the energy transferred into this region. Also the accuracy of the results may be lost if there is an incorrect cutoff in the turbulence production zone.

The boundaries of each spectral bin are defined as:

$$\kappa_m = \xi \kappa_{m-1} = \xi^m \kappa_0 \tag{2}$$

where the parameter ξ sets the spectral resolution of the model (i.e., how well we want to resolve the energy spectrum).

We define the energy bins using a turbulent kinetic energy density function, $E(\kappa)$:

$$k_m = \int_{\kappa_{m-1}}^{\kappa_m} E(\kappa)\,\mathrm{d}\kappa \tag{3}$$

where $E(\kappa)$ is the turbulent kinetic energy density function, κ is the wave number, defined as $\kappa = 2\pi/\lambda$, and λ is a liquid eddy's characteristic length scale.

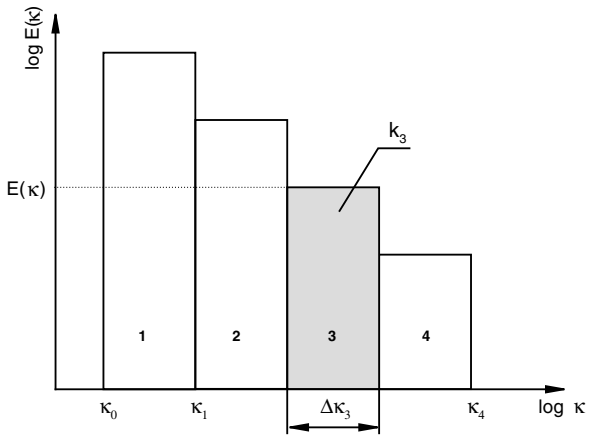

Fig. 2. Turbulent kinetic energy bins, N = 4.

We define every liquid eddy size range by a bin and the energy of those eddies as the bin energy. The next step is to develop an equation for bin energy conservation. As a basis for developing the cascade model's transport equations we use the well-known total turbulent kinetic energy transport equation (e.g., Wilcox, 2002):

$$\frac{Dk}{Dt} \equiv \frac{\partial k}{\partial t} + U_j \frac{\partial k}{\partial x_j} = -\overline{u_i u_j}\frac{\partial U_i}{\partial x_j} - \nu \overline{\frac{\partial u_i}{\partial x_k}\frac{\partial u_i}{\partial x_k}} + \frac{\partial}{\partial x_j}\left[\nu \frac{\partial k}{\partial x_j} - \frac{1}{2}\overline{u_i u_i u_j} - \frac{1}{\rho}\overline{p' u_j}\right] \quad (4)$$

where on the right-hand side we have production, dissipation, molecular diffusion, turbulent transport and pressure diffusion terms, respectively. This equation can be rigorously derived using the Navier–Stokes equations and Reynolds averaging. For the single and two-phase cascade models we assume the Boussinesq approximation is valid since it is normally assumed for most turbulent kinetic energy based models. Following commonly used approximations for the turbulent transport and pressure diffusion terms we rewrite Eq. (4) as,

$$\frac{Dk}{Dt} = \left(2\nu_T S_{ij} - \frac{2}{3}k\delta_{ij}\right)\frac{\partial U_i}{\partial x_j} - \nu \overline{\frac{\partial u_i}{\partial x_k}\frac{\partial u_i}{\partial x_k}} + \frac{\partial}{\partial x_j}\left[\left(\nu + \frac{\nu_T}{\sigma_k}\right)\frac{\partial k}{\partial x_j}\right] \quad (5)$$

where $S_{ij} = \frac{1}{2}(\partial U_i/\partial x_j + \partial U_j/\partial x_i)$ is the mean rate of strain, δ_{ij} is the Kroneker delta function and σ_k is a model constant.

The spectral cascade model involves the same basic components as total turbulent kinetic energy transport equation, Eq. (5). That is, production, dissipation and diffusion. We must also include a spectral transfer term to account for the energy exchange between different wave number bins. Thus, the general form of a single-phase version of the spectral turbulent cascade transport equation for bin-m is (Lewalle and Tavlarides, 1994):

$$\frac{Dk_m}{Dt} = P_m - \varepsilon_m + D_m + T_m \quad (6)$$

where D_m, P_m, ε_m and T_m are the diffusion, production, dissipation and transfer of the turbulent kinetic energy in bin-m, respectively. For the problem being considered herein, the decay of homogeneous turbulent flow, there are no diffusion and production terms since we do not have gradients of mean quantities. That is, the absence of a mean velocity gradient eliminates the production term (P_m) and the turbulent kinetic energy's uniform distribution eliminates the diffusion term (D_m). Thus Eq. (6) reduces to:

$$\frac{Dk_m}{Dt} = T_m - \varepsilon_m \quad (7)$$

The spectral transfer term (T_m) is responsible for the exchange of energies between the adjacent bins. As shown schematically in Fig. 3, we consider the four possible parts of this term: the energy inflows through the left boundary of the bin, the energy outflows through the right boundary as well as the possible outflows through left and inflows through the right boundaries (i.e., a backward cascade):

$$T_m = T^{\mathrm{l}}_{\mathrm{in}} - T^{\mathrm{l}}_{\mathrm{out}} + T^{\mathrm{r}}_{\mathrm{in}} - T^{\mathrm{r}}_{\mathrm{out}} \quad (8)$$

Let us consider the first term in detail. As shown in Fig. 3, at the left boundary the transfer of turbulence occurs with wave number κ_{m-1}. Following a donor-cell type approach and using dimensional analysis, as proposed by Kovasznay (Hinze, 1975), we write the following expression:

$$T^{\mathrm{l}}_{\mathrm{in}} \propto \kappa_{m-1}\left(k_{m-1}\sqrt{E_m \bar{\kappa}_m}\right) \quad (9)$$

Here k_{m-1} is the quantity being transferred from the left bin, $\sqrt{E_m\bar{\kappa}_m}$ is the characteristic speed of the transfer, $E_m = k_m/\Delta\kappa_m$ is the energy density in bin-m, $\Delta\kappa_m = \kappa_m - \kappa_{m-1}$ is the width of wave number bin-m, $\bar{\kappa}_m = 1/2(\kappa_{m-1} + \kappa_m)$ is the characteristic wave number of bin-m, and κ_{m-1} is the wave number associated with the transfer. Similarly, for all other terms we have:

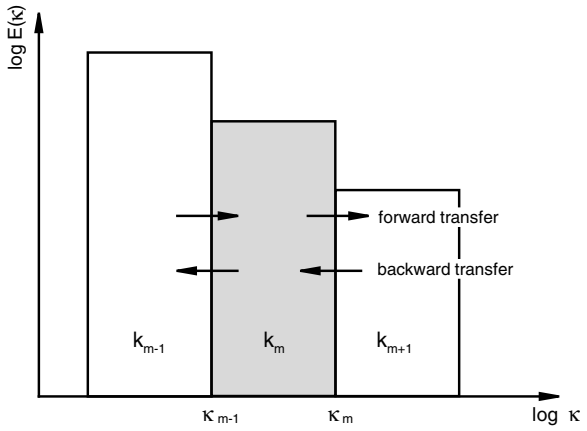

Fig. 3. Spectral transfer of energy between bins (for bin-m).

$$T^{\mathrm{l}}_{\mathrm{out}} \propto \kappa_{m-1}\left(k_m\sqrt{E_{m-1}\bar{\kappa}_{m-1}}\right) \quad (10)$$

$$T^{\mathrm{r}}_{\mathrm{in}} \propto \kappa_m\left(k_{m+1}\sqrt{E_m\bar{\kappa}_m}\right) \quad (11)$$

$$T^{\mathrm{r}}_{\mathrm{out}} \propto \kappa_m\left(k_m\sqrt{E_{m+1}\bar{\kappa}_{m+1}}\right) \quad (12)$$

Introducing proportionality constants, and combining Eqs. (8)–(12), we can write the final expression for the transfer term of bin-m as:

$$T_m = C_1\kappa_{m-1}k_{m-1}\sqrt{E_m\bar{\kappa}_m} - C_1\kappa_m k_m\sqrt{E_{m+1}\bar{\kappa}_{m+1}} - C_2\kappa_{m-1}k_m\sqrt{E_{m-1}\bar{\kappa}_{m-1}} + C_2\kappa_m k_{m+1}\sqrt{E_m\bar{\kappa}_m} \quad (13)$$

where $C_1 = 1.2$ and $C_2 = 0.38$ are model constants which quantify the rate of forward and backward cascade turbulent energy transfer, respectively. As will be discussed in more detail subsequently, the values for C_1 and C_2 were determined from a well-characterized data set (Kang et al., 2003) and then were frozen and used in all subsequent model assessments.

The definition of the transfer term given in Eq. (13) is dimensionally consistent as a source term for the spectral turbulent kinetic energy transport equation. It also satisfies the restriction $\sum_{m=1}^{N} T_m = 0$ which is required to obtain the total turbulent kinetic energy equation by adding together the individual bin energy equations, and, as shown in Appendix A, it implies a $-5/3$ slope in the inertial subrange for single-phase flow in accordance with Kolmogorov's law (Pope, 2000).

A bin's dissipation comes from the following fundamental equation (Pope, 2000):

$$\varepsilon_{(\kappa_a,\kappa_b)} = \int_{\kappa_a}^{\kappa_b} 2\nu\kappa^2 E(\kappa)\,\mathrm{d}\kappa \quad (14)$$

which represents the contribution to the dissipation rate, ε, from turbulent motion in the wave number range (κ_a, κ_b). Thus, in order to obtain the value of the dissipation rate in bin-m, we rewrite Eq. (14) as:

$$\varepsilon_m = \int_{\kappa_{m-1}}^{\kappa_m} 2\nu\kappa^2 E(\kappa)\,\mathrm{d}\kappa \quad (15)$$

We can approximate $E(\kappa)$ in the interval (κ_{m-1}, κ_m) as being a constant, $E(\kappa) \cong k_m/\Delta\kappa_m$, where $\Delta\kappa_m = \kappa_m - \kappa_{m-1}$.

Thus, performing the integration in Eq. (15):

$$\varepsilon_m \cong \int_{\kappa_{m-1}}^{\kappa_m} 2\nu\kappa^2\frac{k_m}{\Delta\kappa_m}\,\mathrm{d}\kappa = 2\nu\frac{k_m}{\Delta\kappa_m}\int_{\kappa_{m-1}}^{\kappa_m}\kappa^2\,\mathrm{d}\kappa$$

$$\varepsilon_m \cong 2\nu \frac{k_m}{\Delta\kappa_m}\frac{\kappa^3}{3}\Big|_{\kappa_{m-1}}^{\kappa_m} = 2\nu\frac{k_m}{\Delta\kappa_m}\left(\frac{\kappa_m^3}{3}-\frac{\kappa_{m-1}^3}{3}\right)$$
$$= \frac{2}{3}\nu\frac{k_m}{\Delta\kappa_m}(\kappa_m-\kappa_{m-1})\left(\kappa_m^2+\kappa_m\kappa_{m-1}+\kappa_{m-1}^2\right)$$

Hence

$$\varepsilon_m \cong \frac{2}{3}\nu k_m\left(\kappa_m^2+\kappa_m\kappa_{m-1}+\kappa_{m-1}^2\right) \tag{16}$$

One of the inherent advantages of using a spectral turbulent cascade model for two-phase flows is the elimination of the empirical dissipation rate transport equation and the capability of adding a bubble energy source term into different energy bins corresponding to the size of the various bubbles (i.e., for polydispersed flows). In this way we can mechanistically model the two-phase energy spectrum through the nonlinear interactions between the bubble-induced and shear-induced liquid eddies of different sizes.

4. Bubble source term

For the case of polydispersed bubbly flow in which there is no bubbly break up and coalescence, we can split the bubbles into N_S size groups. Each of these size groups will have a set of characteristic parameters, such as the volume fraction occupied by the bubbles in that group, the mean diameter of the bubbles and the relative velocity of the bubbles of the group. These parameters will determine how a particular bubble size contributes to the turbulent kinetic energy of the flow and how this energy contribution modifies the energy spectrum of the flow. We assume that linear superposition can be used to compute the influence of all the different size groups on the turbulent kinetic energy spectrum. Since only monodispersed experimental data are available we use only one size group of bubbles in the present work ($N_S = 1$).

Lance and Bataille's (1991) experiments were chosen to validate the performance of the spectral turbulent cascade-transport model since these experimental data are comprehensive, self-consistent, and provide the energy spectrum for decaying single-phase and bubbly two-phase homogeneous grid turbulence.

The bubble source term which was used herein comes from a phenomenological model proposed by Lahey (2005):

$$\Phi_i = C_{p_i}\left(1+C_{D_i}^{4/3}\right)\alpha_i U_{R_i}^3/D_i, \quad (\mathrm{m^2/s^3}) \tag{17}$$

where C_{D_i} is the drag coefficient for a dispersed bubble of size group-i, α_i is the local gas volume (i.e., void) fraction of size group-i, U_{R_i} is relative velocity of size group-i and D_i is the mean bubble diameter of size group-i. This term represents the bubble's total contribution to the induced liquid phase turbulence from a bubble in size group-i (i.e., the pseudo-turbulence due to liquid displacement by the bubbles and their wakes). The bubble-induced turbulence is distributed among the various wave number bins as described later in the paper. It should be noted that Eq. (17) has only been verified (Lahey, 2005) for bubbly two-phase flows with bubble diameters ranging from about 1.0 to 5.0 mm.

The following empirical expression was used for the value of the parameter C_{p_i}:

$$C_{p_i} = b_1 + (b_2 Ku_i - b_3)\alpha_i^2 \tag{18}$$

where $Ku_i = \frac{(U_L+U_{R_i})\rho_L^{1/2}}{[\sigma g(\rho_L-\rho_G)]^{1/4}}$ is the Kutateladze number, $b_1 = 0.045$, $b_2 = 65.0$, $b_3 = 195.0$, U_L is the mean liquid phase velocity, ρ_L and ρ_G are the liquid and gas phase densities, respectively, and σ is the surface tension. The set of the Kutateladze numbers and the resulting C_{p_i} dependences for the experiments which were considered herein are given in Table 1.

Table 1
C_p and Kutateladze number (Ku) dependence on mean liquid velocity, U_L, for $D_b = 5$ mm

U_L (m/s)	Ku	C_p
0.4	3.85	$0.045 + 55\alpha^2$
0.5	4.46	$0.045 + 95\alpha^2$
0.6	5.08	$0.045 + 135\alpha^2$
0.8	6.30	$0.045 + 215\alpha^2$
0.9	6.91	$0.045 + 255\alpha^2$

Interestingly, Ruggles et al. (1988) found a very similar functional form for the virtual volume coefficient,

$$C_{VM_i} = c_1(1+c_2\alpha_i^2) \tag{19}$$

and, from potential flow theory, we know that for an immersed sphere (Drew and Passman, 1998), $C_{p_i} = 1/2C_{VM_i}$.

It should be noted that the empirical expression given in Eq. (18) implicitly accounts for non-spherical bubble shapes, bubble interactions and the observed complicated trajectories of the bubbles in the experiments of Lance and Bataille (1991).

In order to evaluate the drag coefficient (C_{D_i}) dependence upon void fraction for the two-phase flow under consideration we used a distorted fluid particle regime correlation for bubbly flows (Ishii and Hibiki, 2006):

$$C_{D_i}(\alpha_i) = \frac{\sqrt{2}}{3}N_\mu N_{Re_i}\left(\frac{1+17.67(1-\alpha_i)^{1.3}}{18.67(1-\alpha_i)^{1.5}}\right)^2 \tag{20}$$

where $N_{Re_i} \equiv \frac{D_i\rho_L|U_{R_i}|}{\mu_c}$, $N_\mu \equiv \mu_c \Big/ \left(\rho_L\sigma\sqrt{\frac{\sigma}{g\Delta\rho}}\right)^{\frac{1}{2}}$. Here D_i is the diameter of the dispersed bubbles in size group-i, μ_c is liquid's dynamic viscosity, σ is the surface tension, and $\Delta\rho = \rho_L - \rho_G$ is the density difference between the liquid and gas phases.

For terminal rise conditions there is a balance between the drag and buoyancy force for a rising bubble in stagnant fluid and we can derive the following relative velocity dependence on drag coefficient:

$$U_{R_i}(\alpha_i) = \sqrt{\frac{4D_i g\Delta\rho}{3\rho_L C_{D_i}(\alpha_i)}} \tag{21}$$

Thus, we have a coupled system of equations, Eqs. (20) and (21), to determine the drag coefficient and the relative velocity dependence on void fraction. Typical results for atmospheric pressure air/water flows are given in Table 2.

5. Mesh independence of wave number bins

The spectral cascade-transport turbulence model allows for different resolution in wave number space. In order to achieve consistent results when using different wave number mesh resolutions we have to implement this into the model. It is known that strong interactions occur mostly between the liquid eddies of similar sizes (Pope, 2000). In particular, more than 75% of the energy exchange happens within the $\frac{1}{2}\kappa$ to 2κ range of eddy sizes for a given wave

Table 2
Relative velocity (U_R) and drag coefficient (C_D) dependence upon void fraction (α), for $D_b = 5$ mm

α (%)	C_D	U_R (m/s)
0.01	1.229	0.2307
0.5	1.231	0.2305
1.0	1.233	0.2303
1.5	1.235	0.2301
2.0	1.238	0.2298
2.5	1.240	0.2296
3.0	1.242	0.2294

number, κ. Eqs. (8)–(13) are thus suitable for the case of $\xi = 2$ (see Eq. (2)). In contrast, if we choose a finer wave number mesh for a given wave number, κ, we have to account for interactions not only between neighboring bins, but also among all the other bins in the range of $\frac{1}{2}\kappa$ to 2κ.

We may assume the following form of an energy transfer term in bin-m for the case $\xi \neq 2$:

$$T_{\text{in}}^{\text{l}} \propto \sum_{j=1}^{N_n} \beta_j \kappa_{m-1} k_{m-j} \sqrt{E_m \bar{\kappa}_m} \tag{22}$$

where N_n is the number of neighbor bins with $\kappa \geqslant 0.5\kappa_m$ (since we are considering only energy transfers from the left bins in this term) and β_j is assumed to be a set of weights having a Gaussian distribution in the logarithmic scale.

The weights, β_j, were computed by averaging the following distribution function over a wave number bin:

$$f(\kappa) = \frac{1}{\hat{\sigma}\sqrt{2\pi}} \exp\left(-\frac{[\log(\kappa) - \log(\bar{\kappa})]^2}{2\hat{\sigma}^2}\right) \tag{23}$$

where $\hat{\sigma} = 0.225$ is the standard deviation and $\bar{\kappa}$ is the left or right boundary of the interacting bin, depending on the direction of the interaction. The value of σ was chosen in such way that 75% of the total spectral interaction of wave number κ would occur with wave numbers p in the range (Domaradzki and Rogallo, 1990), $\kappa/2 \leqslant p \leqslant 2\kappa$.

Let us consider an interaction between bin-m and bin-$m-j$. The following integral is used to compute the weight:

$$\beta_{-j} = \int_{\kappa_{m-j-1}}^{\kappa_{m-j}} \frac{1}{\hat{\sigma}\sqrt{2\pi}} \exp\left(-\frac{[\log(\kappa) - \log(\kappa_{m-1})]^2}{2\hat{\sigma}^2}\right) \mathrm{d}\kappa \tag{24}$$

Here we used equal to the left boundary of the bin-m, κ_{m-1}, since the interacting bin $(m-j)$ is located to the left of the bin-m. The integration is performed over bin-$m-j$ and the integral does not depend on m if the log-uniform scaling of the wave number mesh is used.

Table 3 tabulates a typical set of weight coefficients. Negative values of j designate the location of a neighbor bin on the left of a current bin, and positive values correspond to the neighbor bin on the right. For example, if we want to compute the weighting of the contribution of the spectral transfer term to bin-10 from bin-8, we use $j = -2$. Including the other three components of the spectral transfer term we obtain a generalization of Eq. (13):

$$\begin{aligned} T_m = {} & C_1 \sum_{j=-N_n}^{-1} \beta_j \kappa_{m-1} k_{m+j} \sqrt{E_m \bar{\kappa}_m} - C_1 \sum_{j=1}^{N_n} \beta_j \kappa_{m-1+j} k_m \\ & \times \sqrt{E_{m+j} \bar{\kappa}_{m+j}} - C_2 \sum_{j=-N_n}^{-1} \beta_j \kappa_{m+j} k_m \sqrt{E_{m+j} \bar{\kappa}_{m+j}} + C_2 \\ & \times \sum_{j=1}^{N_n} \beta_j \kappa_m k_{m+j} \sqrt{E_m \bar{\kappa}_m} \end{aligned} \tag{25}$$

Table 3
Sample distribution coefficients β_j for the case of $\xi = 1.37$ (note, $\beta_j = \beta_{-j}$)

j	β_j
−5	0.007
−4	0.029
−3	0.080
−2	0.159
−1	0.224
1	0.224
2	0.159
3	0.080
4	0.029
5	0.007

In summary, in Eq. (25) we use the weights β_j (Table 3) required to ensure the cascade-transport model's independence of the wave number grid.

In order to verify that the energy leaving bin-m_0 arrives at bin-$m_1 = m_0 + j$ in the forward transfer process we can compute the corresponding components of the transfer terms for the considered bins. Using one component of the right boundary's outflow term in Eq. (25) for bin-m_0 we write:

$$T_{m_0}^{m_1} = -C_1 \beta_j \kappa_{m_0-1+j} k_{m_0} \sqrt{E_{m_0+j} \bar{\kappa}_{m_0+j}} \tag{26}$$

The left boundary inflow for the bin-m_1 can be written as:

$$T_{m_1}^{m_0} = C_1 \beta_{-j} \kappa_{m_1-1} k_{m_1-j} \sqrt{E_{m_1} \bar{\kappa}_{m_1}} \tag{27}$$

Noting that $\beta_j = \beta_{-j}$ we can conclude that $T_{m_0}^{m_1} = -T_{m_1}^{m_0}$ and hence, as required, Eq. (25) satisfies pair-wise energy conservation.

Note that both Eqs. (13) and (25) are developed in such a way as to satisfy the required constraint that the sum of all the spectral components of the transfer term does not contribute to the total turbulent kinetic energy. That is,

$$\sum_{m=1}^{N} T_m = 0 \tag{28}$$

The turbulent wake behind a bubble may also introduce turbulent energy into the flow (Lance and Bataille, 1991). As can be seen from experiments (Veldhuis et al., 2005), the sizes of the turbulent liquid eddies in the bubble's wake range from the bubble size down to very small liquid eddies, possibly close to the Kolmogorov scale. The generalization of Eq. (7) for the decay of homogeneous, isotropic bubbly flows is:

$$\frac{Dk_m}{Dt} = T_m - \varepsilon_m + S_m \tag{29}$$

where $S_m = \sum_{i=1}^{N_S} \gamma_{m_i} \Phi_i$ is the sum of contributions from the bubbles of various size groups-i, to wave number bin-m; γ_{m_i} is the weight of the bubble's contribution, for a bubble in size group-i, to the turbulent kinetic energy spectrum in bin-m. These weighting factors are shown in Fig. 4, where $\sum_{m=1}^{N} \gamma_{m_i} = 1$ for all size groups, $i = 1, \ldots, N_S$. Fig. 4 also shows the spectral distribution of the various terms in Eq. (29) for 24 wave number bins and a monodispersed bubbly flow (i.e., $N_S = 1$). We note that the various terms are balanced. The wave number axis has been normalized with the bubble's diameter such that we add most of the bubble's energy between $\kappa D_b = 1$ and the Kolmogorov length scale.

Note that the shape of the bubble source term's distribution (green[1] circles/line in Fig. 4) ensures consistency with the observed slopes in the measured turbulent kinetic energy spectrum, as noted previously, and the bubble source term has a peak at $\kappa D_b = 1$. In particular, in the "inertial subrange" the bubble source spectral density decays as $\kappa^{-1/4}$ while in the dissipation range the decay rate changes to κ^{-1}. Ilic et al. (2007) found from a DNS of bubble-driven liquid flows that for the case of bubble-dominated turbulence the predicted energy spectrum slope is -1 in the high frequency range. Assuming that the bubbles in grid-generated turbulence give the same spectral contribution to the liquid turbulent energy we use this slope in the dissipation range for the bubble's source term. The choice of the $\kappa^{-1/4}$ and $\kappa - 1$ slopes results in an energy spectrum which is in agreement with the slopes (i.e., $-7/6$ and $-11/3$) in two-phase data sets (Lance and Bataille, 1991; Lance, 1979), as will be discussed subsequently.

[1] For interpretation of the references to color in Fig. 4, the reader is referred to the web version of this paper.

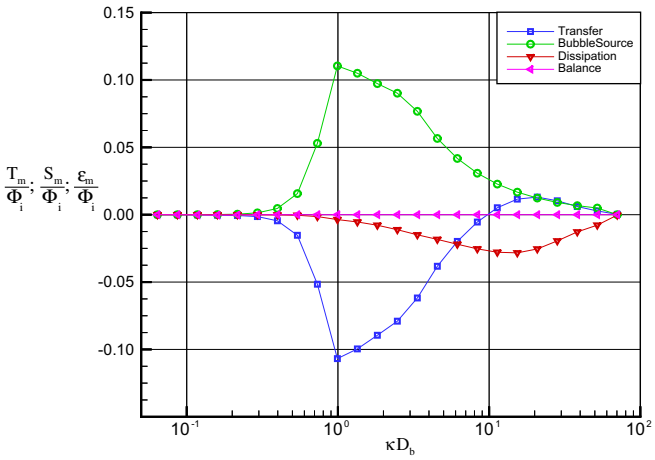

Fig. 4. Spectral distribution of the various spectral terms for the decaying homogeneous, isotropic bubbly two-phase turbulent flow ($\alpha = 1.0\%$) at $U_L = 0.9$ m/s and $X/M = 500$ (experimental conditions of Lance and Bataille (1991)) non-dimensionalized by total bubble source term, Eq. (17), for $D_b = 5$ mm.

6. Model assessment

Kang et al. (2003) measured the decay of active-grid-generated single-phase isotropic turbulence at relatively high Reynolds number (i.e., $Re_\lambda = 720$). They provided spectral information of the turbulent kinetic energy during decay, and these single-phase data have been used to assess our cascade model. We used the turbulent kinetic energy spectrum at the first measuring station ($X/M = 20$) as an initial condition for the turbulent cascade model. The results of the simulation compared to the data of Kang et al. (2003) are given in Fig. 5 (the cascade model used 24 wave number bins to represent the spectrum). We see excellent agreement between the cascade model and these data.

To further assess the model's performance the data of Lance and Bataille (1991) was also used. These data are from a series of experiments on decaying homogeneous, isotropic single and bubbly two-phase grid-generated turbulence, which were performed over a range of void fractions from 0% to 3% and at mean liquid velocities ranging between 0.4 and 0.9 m/s. The turbulent intensity, u'/U_L, was measured at four axial locations, X (normalized with respect to the mesh spacing M), downstream of turbulence-generating grid: $X/M = 21.4$, 31.4, 36.4 and 51.4. The results for various mean velocities, U_L, were given by Lance (1979). Significantly, Lance and Bataille (1991) observed that in their experiments the isotropy of the initial turbulent field was not changed by the injection of the air bubbles. Thus, the spectral cascade model, which was developed under assumption of isotropy, is also applicable to the two-phase bubbly flows considered by Lance and Bataille (1991).

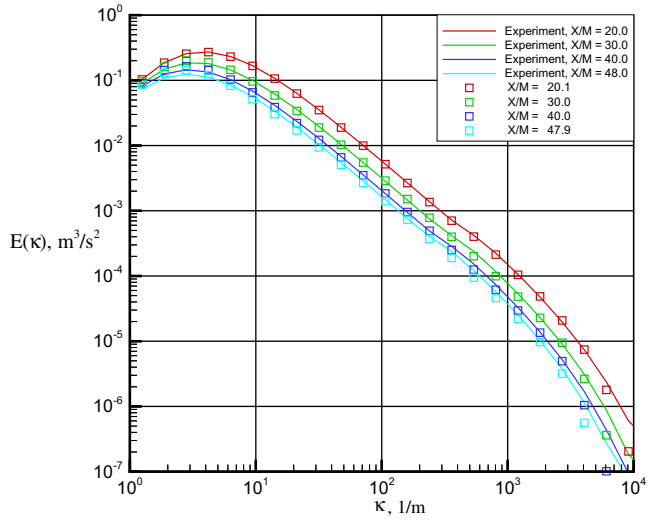

Fig. 5. Turbulent kinetic energy spectra at different measuring stations. Data of Kang et al. (2003), (lines), compared to single-phase cascade model results, (symbols).

Fig. 1 shows the single and two-phase energy spectra reported by Lance and Bataille (1991). We can observe a $-5/3$ slope in the inertial subrange and -5 slope in the dissipation range for turbulent single-phase flow. For turbulent two-phase flows the equivalent[2] "inertial subrange" slope is about $-7/6$ and the equivalent[2] "dissipation region" is about $-11/3$, having a relatively small region with a $-8/3$ slope. There is no sharp transition from $-5/3$ to $-8/3$ or $-11/3$, however, as can be seen, all those slopes can be found in different ranges of the turbulent kinetic energy spectrum. As noted previously, Bunner and Tryggvason (2003) also observed a $-3.6 \approx -11/3$ slope in their DNS results for turbulent deformable bubbly flow.

In order to specify the initial conditions for the spectral cascade model simulations of Lance and Bataille's (1991) experiments we used the functional form of the 3-D turbulent kinetic energy spectrum given by Kang et al. (2003):

$$E(\kappa) = c\varepsilon^{2/3}\kappa^{-5/3}\left[\frac{\kappa\Lambda}{\left[(\kappa\Lambda)^{a_2} + a_1\right]^{1/a_2}}\right]^{5/3+a_3} e^{-a_4\kappa\eta} \tag{30}$$

The procedure described in Kang et al. (2003) was used to obtain the coefficients in Eq. (30), $c = 8.0$, $a_1 = 0.39$, $a_2 = 1.2$, $a_3 = 12.0$, $a_4 = 5.0$, and the following flow parameters were used: integral length scale, $\Lambda = 0.02$ m, Kolmogorov scale, $\eta = 5.3 \times 10^{-4}$ m, turbulent dissipation rate, $\varepsilon = 0.004$ m^2/s^3.

An analytical formula given by Pope (2000) was used to convert the 3-D energy spectrum (E), in Eq. (30), into the corresponding 1-D energy spectrum (E_{11}) so that it could be compared directly with Lance and Bataille's (1991) results:

$$E_{11}(\kappa_1) = \int_{\kappa_1}^{\infty} \frac{E(\kappa)}{\kappa}\left(1 - \frac{\kappa_1^2}{\kappa^2}\right)d\kappa \tag{31}$$

Fig. 6 shows the predicted 1-D energy spectra for both single and two-phase flows at $U_L = 0.9$ m/s, for a mean air bubble diameter of $D_b = 5.0$ mm. The turbulent kinetic energy density was non-dimensionalized with respect to the mean turbulence level, so that all the spectra could be compared on the same scale (i.e., using the same scaling as was used by Lance and Bataille (1991)). The predicted single-phase energy spectrum (the red[3] circles/line in Fig. 6) shows the well-known $-5/3$ slope in the inertial transfer range and a -5 slope in the dissipation range, while the predicted two-phase spectra for void fractions between 0.5% and 3.0%, show a $-7/6$ slope in the equivalent "inertial subrange" and a $-11/3$ slope in the equivalent "dissipation region". As noted in Fig. 1, these slopes can be observed in the data of Lance and Bataille (1991) and have also been seen by others in their experiments. Thus, the cascade model appears to be capable of predicting the observed energy density spectrum for decaying homogeneous, isotropic turbulent single and two-phase bubbly flows.

Figs. 7 and 8 show the spatial evolution of the turbulent intensity compared to the data of Lance and Bataille (1991) and Lance (1979), respectively, where the turbulent intensity was defined as:

[2] Due to bubble-induced turbulence, in bubbly two-phase flows there is no pure inertial subrange and dissipation region as in single-phase turbulent flows.

[3] For interpretation of the references to color in Fig. 6, the reader is referred to the web version of this paper.

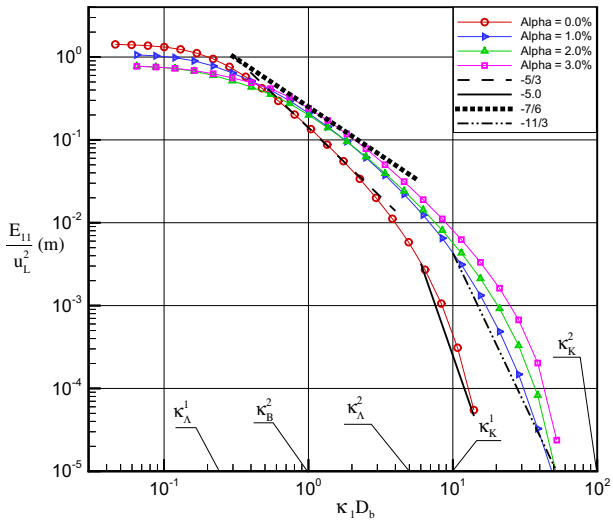

Fig. 6. Cascade-transport model predictions of the one-dimensional turbulent kinetic energy spectra (E_{11}) and different slopes for void fractions from 0.0% to 3.0% at a mean liquid velocity of 0.9 m/s, for D_b = 5 mm. The various scales shown are as in Fig. 1.

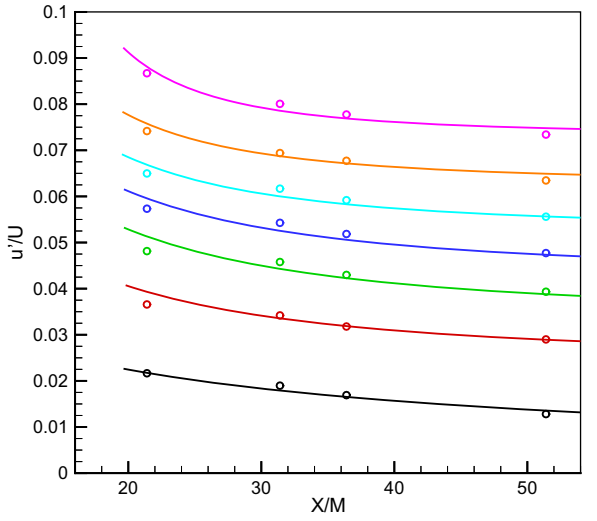

Fig. 7. Turbulent intensity vs. normalized test section length from the grid. Cascade-transport model results (lines) compared to Lance and Bataille's (1991) experimental data for U_L = 0.6 m/s. The void fraction (α) varies from 0.0% to 3.0% in 0.5% increments (from bottom to top).

$$\frac{u'}{U_L} \equiv \frac{\sqrt{2k/3}}{U_L} = \frac{\sqrt{(u'^2+v'^2+w'^2)/3}}{U_L} \tag{32}$$

Here k is the total turbulent kinetic energy of the liquid and $U \equiv U_L$ is the mean liquid velocity of the one-dimensional grid generated turbulent flow. The scale of the abscissa is normalized by the grid mesh spacing, M = 0.04 m, used in the experiments of Lance and Bataille (1991) and Lance (1979).

It should be noted that because of the characteristics of the intrusive hot film probe which was used in these experiments the larger the mean flow velocity, U_L, the more reliable the two-phase data. That is, because of surface tension, at low mean liquid velocities, a hot film probe has a more difficult time penetrating the bubbles and they may not cleanly detach from it, both of which may adversely affect the measurements.

Anyway, as can be seen, the turbulent cascade-transport model shows good agreement with the experimental data over a wide range of flow parameters. Moreover, as expected, the liquid turbulence level increases as void fraction increases. Thus it appears that, unlike non-spectral two-equation turbulent kinetic energy transport models, bubble-induced and shear-induced turbulence production mechanisms can be superimposed in a spectral turbulent cascade transport model even for larger void fractions (i.e., $\alpha > 2\%$).

Indeed, Lance and Bataille (1991) observed an interesting non-linear behavior of the excess (i.e., the bubble-induced) turbulent kinetic energy with respect to void fraction. Previous non-spectral two-phase k–ε models (Lahey, 2005) were unable to predict this behavior. Fig. 9 shows spectral cascade model predictions and the data for various levels of fluctuations generated by the grid (u'_0/U_R). As Lance and Bataille (1991) noted, below some critical void fraction, α_c, the behavior of the non-dimensional excess turbulent kinetic energy (i.e., u'^2_E/U^2_R, where $u'^2_E \equiv u'^2 - u'^2_0$; u'^2_0 and u'^2 are the single and two-phase turbulent kinetic energies, respectively) does not depend upon the grid-generated turbulent intensity. Moreover, for $\alpha < \alpha_c$, the excess turbulent kinetic energy increases linearly with void fraction (α). In contrast, for void fractions above this critical value there is a strong dependence on u'_0/U_R. Previous two-phase models (Lahey, 2005; Nigmatulin, 1979) were unable to predict this non-linear phenomenon due to their linear, or near linear, void fraction dependence and thus, at best, these models were accurate only for low void fractions (i.e., $\alpha < \alpha_c$).

In particular, let us consider the bubble-induced turbulence model of Nigmatulin (1979) for monodispersed bubbly flow:

$$\underline{\tau}^T_{cl(PI)} = a_{cl}\alpha\rho_{cl}\left[3\underline{\mathbf{U}}_R \cdot \underline{\mathbf{U}}_R\underline{\mathbf{I}} + \underline{\mathbf{U}}_R\underline{\mathbf{U}}_R\right] \tag{33}$$

where for spherical bubbles, a_{cl} = 1/20. Assuming that the mean relative velocity vector's only non-zero component is stream-wise (i.e., $\underline{\mathbf{U}}_R = [U_R, 0, 0]$), we can compute the bubble-induced turbulent kinetic energy by taking the trace of Eq. (33):

$$u'^2_E \equiv \langle u_i u_i \rangle^E = a_{cl}\alpha\left[\mathrm{trace}(3\underline{\mathbf{U}}_R \cdot \underline{\mathbf{U}}_R\underline{\mathbf{I}}) + U^2_R\right] = a_{cl}\alpha[9U^2_R + U^2_R] = \frac{1}{2}\alpha U^2_R \tag{34}$$

Thus, the non-dimensional excessive turbulent kinetic energy based on Nigmatulin (1979) model of bubble-induced turbulence is:

$$\left.\frac{u'^2_E}{U^2_R}\right|_N = \frac{1}{2}\alpha \tag{35}$$

Let us next consider this dependence for the bubble source model that we have used (Eq. (17)). Lopez de Bertodano (1992) proposed the following first-order relaxation transport equation for bubble-induced turbulence:

$$\alpha_{cl}\frac{Dk_b}{Dt} = \nabla \cdot \alpha_{cl}\nu^T\nabla k_b + \frac{1}{\tau_b}(k_{ba} - k_b) \tag{36}$$

where α_{cl} is liquid phase volume fraction ($\alpha_{cl} = 1 - \alpha$), k_{ba} is the asymptotic value of the bubble's kinetic energy, and τ_b is a relaxation time for the bubble's energy transfer to the liquid turbulence:

$$\tau_b = \frac{D_b}{U_R} \tag{37}$$

Since the last term in Eq. (36) represents the bubble source term we can write, using Eqs. (36) and (17):

$$\frac{1}{\tau_b}(k_{ba} - k_b) = C_p(1 + C_D^{4/3})\alpha(1-\alpha)U^3_R/D_b \tag{38}$$

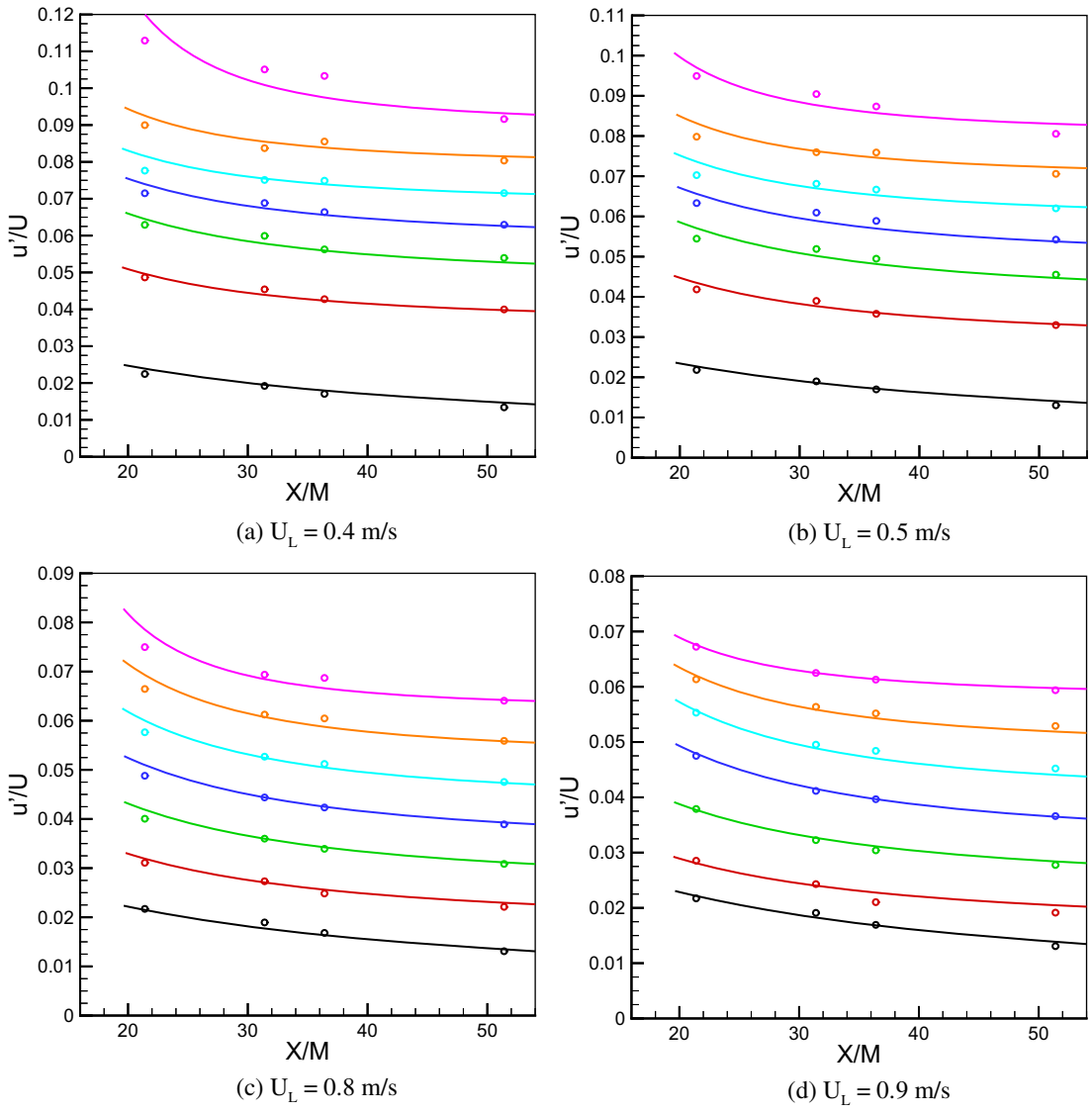

Fig. 8. Turbulence level evolution for different mean liquid velocities; cascade model comparisons with the data of Lance (1979). The void fraction (α) values from 0% to 3% in 0.5% increments (from bottom to top of each plot).

Using Eq. (37) we conclude:

$$k_{ba} - k_b = C_p(1 + C_D^{4/3})\alpha(1-\alpha)U_R^2 \tag{39}$$

Thus, since for atmospheric pressure air/water bubbly flows the kinetic energy of the bubbles and the liquid are strongly coupled (Drew and Passman, 1998), the excess of turbulent kinetic energy implied by the bubble source term in Eq. (17) for monodispersed bubbly flow is:

$$\left.\frac{u_E'^2}{U_R^2}\right|_L = 2C_p(1 + C_D^{4/3})\alpha(1-\alpha) = \frac{1}{2}(1 + C_D^{4/3})\alpha(1-\alpha) \tag{40}$$

where $C_p = 0.25$ for a spherical bubble (Drew and Passman, 1998).

Fig. 9 shows the comparison between the Nigmatulin (1979), Eq. (35), and Lahey (2005), Eq. (40), non-spectral bubble-induced turbulence models, the experimental data of Lance and Bataille (1991) and the spectral cascade model's predictions. For the range of void fractions of interest, both Nigmatulin's and Lahey's non-spectral models show a nearly linear dependence with void fraction on the bubble-induced turbulent kinetic energy of the liquid. As can be noted, at higher void fractions (α) these models fail to predict the non-linear behavior of the bubble-induced turbulence energy. In contrast, when using Eq. (17) within the spectral turbulent cascade model one is able to predict these data. That is, the observed non-linear dependence on void fraction is predicted when the effect of the bubble(s) is introduced into the appropriate spectral bin.

An additional advantage of spectral modeling is the opportunity to analyze polydispersed bubbly flows. The ability to introduce source terms into the proper scales of turbulence makes the spectral cascade model a better choice over classical two-equation (e.g., k–ε) models for use in multiphase flow modeling.

7. Conclusions

The spectral turbulent cascade-transport model presented herein predicts single and bubbly two-phase flows over a fairly wide range of flow conditions. In particular, it properly predicts the energy spectrum evolution in both the wave number and spatial domains for decaying homogeneous, isotropic turbulent flows.

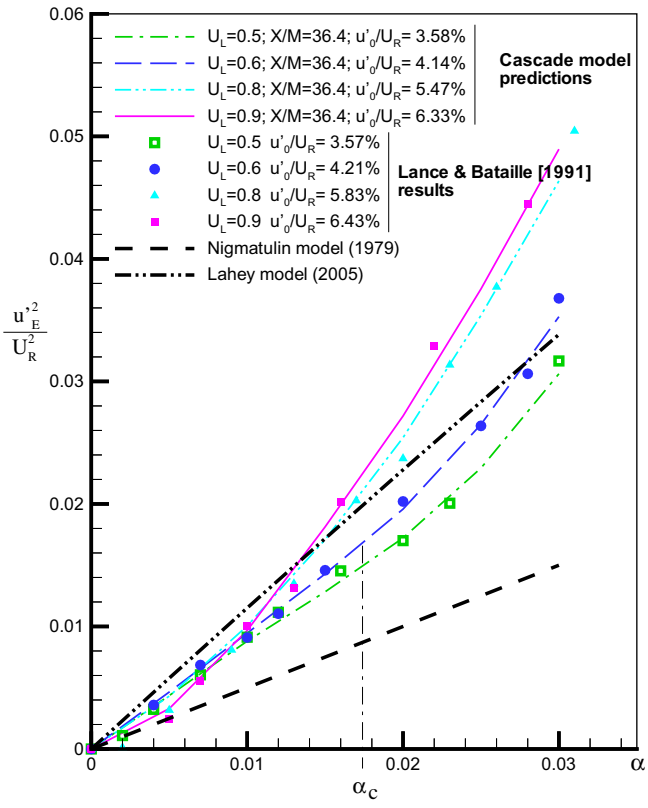

Fig. 9. Cascade model predictions (lines) of the excess relative kinetic energy dependence on void fraction (α) for different values of grid-generated turbulence compared to experimental data of Lance and Bataille (1991), (symbols), and the non-spectral bubble-induced turbulence models of Lahey (2005) and Nigmatulin (1979), (bold line plots).

Acknowledgements

The authors acknowledge the support given this study by the National Science Foundation (NSF) and the Office of Naval Research (ONR). In addition, we acknowledge Professors Charles Meneveau and Andrea Prosperetti (Johns Hopkins University) who first made us aware of the potential of the spectral cascade modeling approach for turbulent two-phase flows, and Professor Stephen Pope (Cornell University) for his many helpful suggestions.

Appendix A. Energy spectrum's slope derivation based on the spectral cascade model equations

Consider the inertial subrange of a single-phase turbulence kinetic energy spectrum. In this range we do not have any significant contribution from either viscous dissipation or energy production. Thus, using Eq. (7), we can write the equation for evolution of energy in this range as:

$$\frac{dk_p}{dt} \cong T_p \tag{A.1}$$

where

$$T_p = C_1\kappa_{p-1}k_{p-1}(E_p\kappa_p)^r - C_1\kappa_p k_p(E_{p+1}\kappa_{p+1})^r \tag{A.2}$$

is the spectral transfer term in the forward direction, and from Eq. (9), $r = \frac{1}{2}$.

In order to determine the slope of the turbulent energy spectrum we make the following assumptions:

- We may have a constant slope "$-s$" in a particular range of wave number space:

$$E(\kappa) = A(t)\kappa^{-s} \tag{A.3}$$

- The function $A(t)$ depends only upon time, so the decay rate is the same anywhere in the inertial subrange.
- The wave number mesh is uniform in the log-scale:

$$\kappa_{p+1} = \lambda\kappa_p \tag{A.4}$$

Consider three wave number bins in the inertial range and compute the turbulent kinetic energy in these bins using Eq. (A.3):

$$k_p = \int_{\kappa_{p-1}}^{\kappa_p} A(t)\kappa^{-s}\,d\kappa = \frac{A(t)}{1-s}\left[\kappa_p^{1-s} - \kappa_{p-1}^{1-s}\right], \quad p = m-1,\ldots,m+1 \tag{A.5}$$

The rate of transfer coefficient can be expressed as:

$$E_p\bar{\kappa}_p = \frac{k_p}{\Delta\kappa_p}\bar{\kappa}_p = \frac{A(t)}{1-s}\left[\kappa_p^{1-s} - \kappa_{p-1}^{1-s}\right]\frac{\bar{\kappa}_p}{\Delta\kappa_p}, \quad p = m-1,\ldots,m+1 \tag{A.6}$$

Using Eq. (A.4) we can show that the last multiplier does not depend on p:

$$\frac{\bar{\kappa}_p}{\Delta\kappa_p} = \frac{\frac{1}{2}(\kappa_{p-1}+\kappa_p)}{\kappa_p - \kappa_{p-1}} = \frac{\frac{1}{2}\kappa_0(\lambda^{p-1}+\lambda^p)}{\kappa_0(\lambda^p - \lambda^{p-1})} = \frac{1}{2}\frac{\lambda+1}{\lambda-1}, \quad p = m-1,\ldots,m+1 \tag{A.7}$$

Introducing $\xi = \frac{1}{2}\frac{\lambda+1}{\lambda-1}$ we can rewrite the rate of transfer coefficient as:

$$E_p\bar{\kappa}_p = \frac{A(t)\xi}{1-s}\left[\kappa_p^{1-s} - \kappa_{p-1}^{1-s}\right], \quad p = m-1,\ldots,m+1 \tag{A.8}$$

Substituting Eq. (A.5) into Eq. (A.1) for $p = m$ and $p = m+1$:

$$\begin{aligned}\frac{dA(t)}{dt}\frac{\kappa_m^{1-s} - \kappa_{m-1}^{1-s}}{1-s} &= T_m \\ \frac{dA(t)}{dt}\frac{\kappa_{m+1}^{1-s} - \kappa_m^{1-s}}{1-s} &= T_{m+1}\end{aligned} \tag{A.9}$$

Eqs. (A.9) can be combined to obtain:

$$T_{m+1}\left(\kappa_m^{1-s} - \kappa_{m-1}^{1-s}\right) = T_m\left(\kappa_{m+1}^{1-s} - \kappa_m^{1-s}\right) \tag{A.10}$$

Using Eq. (A.2) we can rewrite (A.10) as:

$$\begin{aligned}&\left(C_1\kappa_m k_m E_{m+1}^r\kappa_{m+1}^r - C_1\kappa_{m+1}k_{m+1}E_{m+2}^r\kappa_{m+2}^r\right)\left(\kappa_m^{1-s} - \kappa_{m-1}^{1-s}\right) \\ &= \left(C_1\kappa_{m-1}k_{m-1}E_m^r\kappa_m^r - C_1\kappa_m k_m E_{m+1}^r\kappa_{m+1}^r\right)\left(\kappa_{m+1}^{1-s} - \kappa_m^{1-s}\right)\end{aligned} \tag{A.11}$$

Eqs. (A.5) and (A.8) can be used to eliminate the bin turbulent kinetic energies from Eq. (A.11):

$$\begin{aligned}&\begin{pmatrix}\kappa_m\left[\kappa_m^{1-s} - \kappa_{m-1}^{1-s}\right]\left[\kappa_{m+1}^{1-s} - \kappa_m^{1-s}\right]^r\xi^r \\ -\kappa_{m+1}\left[\kappa_{m+1}^{1-s} - \kappa_m^{1-s}\right]\left[\kappa_{m+2}^{1-s} - \kappa_{m+1}^{1-s}\right]^r\xi^r\end{pmatrix}\left(\kappa_m^{1-s} - \kappa_{m-1}^{1-s}\right) \\ &= \begin{pmatrix}\kappa_{m-1}\left[\kappa_{m-1}^{1-s} - \kappa_{m-2}^{1-s}\right]\left[\kappa_m^{1-s} - \kappa_{m-1}^{1-s}\right]^r\xi^r \\ -\kappa_m\left[\kappa_m^{1-s} - \kappa_{m-1}^{1-s}\right]\left[\kappa_{m+1}^{1-s} - \kappa_m^{1-s}\right]^r\xi^r\end{pmatrix}\left(\kappa_{m+1}^{1-s} - \kappa_m^{1-s}\right)\end{aligned} \tag{A.12}$$

Let us next use Eq. (A.4) to rewrite the wave numbers as:

$$\kappa_{m-2} \equiv x; \quad \kappa_{m-1} = \lambda x; \quad \kappa_m = \lambda^2 x; \quad \kappa_{m+1} = \lambda^3 x; \quad \kappa_{m+2} = \lambda^4 x \tag{A.13}$$

Thus, Eq. (A.12), expressed in terms of λ, x and s, becomes:

$$\begin{pmatrix} (\lambda^2 x)\left[(\lambda^2 x)^{1-s}-(\lambda x)^{1-s}\right]\left[(\lambda^3 x)^{1-s}-(\lambda^2 x)^{1-s}\right]^r \\ -(\lambda^3 x)\left[(\lambda^3 x)^{1-s}-(\lambda^2 x)^{1-s}\right]\left[(\lambda^4 x)^{1-s}-(\lambda^3 x)^{1-s}\right]^r \end{pmatrix}\left((\lambda^2 x)^{1-s}-(\lambda x)^{1-s}\right)$$
$$= \begin{pmatrix} (\lambda x)[(\lambda x)^{1-s}-x^{1-s}]\left[(\lambda^2 x)^{1-s}-(\lambda x)^{1-s}\right]^r \\ -(\lambda^2 x)\left[(\lambda^2 x)^{1-s}-(\lambda x)^{1-s}\right]\left[(\lambda^3 x)^{1-s}-(\lambda^2 x)^{1-s}\right]^r \end{pmatrix}\left((\lambda^3 x)^{1-s}-(\lambda^2 x)^{1-s}\right)$$

Next let us divide through by, $[(\lambda x)^{1-s}-x^{1-s}]((\lambda^2 x)^{1-s}-(\lambda x)^{1-s})$:

$$\left((\lambda^2 x)\lambda^{1-s}\left[(\lambda^3 x)^{1-s}-(\lambda^2 x)^{1-s}\right]^r-(\lambda^3 x)(\lambda^2)^{1-s}\left[(\lambda^4 x)^{1-s}-(\lambda^3 x)^{1-s}\right]^r\right)$$
$$=\left((\lambda x)\left[(\lambda^2 x)^{1-s}-(\lambda x)^{1-s}\right]^r-(\lambda^2 x)\lambda^{1-s}\left[(\lambda^3 x)^{1-s}-(\lambda^2 x)^{1-s}\right]^r\right)\lambda^{1-s} \tag{A.14}$$

Dividing Eq. (A.14) by $x[(\lambda^2 x)^{1-s}-(\lambda x)^{1-s}]^r$ we obtain:

$$\left((\lambda^2)\lambda^{1-s}[\lambda^{1-s}]^r-(\lambda^3)(\lambda^2)^{1-s}[(\lambda^2)^{1-s}]^r\right)$$
$$=\left((\lambda)-(\lambda^2)\lambda^{1-s}[\lambda^{1-s}]^r\right)\lambda^{1-s} \tag{A.15}$$

Thus for the powers of λ:

$$\lambda^{3+r-s(1+r)}-\lambda^{5+2r-s(2+2r)}=\lambda^{2-s}-\lambda^{4+r-s(2+r)} \tag{A.16}$$

Dividing Eq. (A.16) by λ^{2-s}:

$$\lambda^{1+r-sr}-\lambda^{3+2r-s(1+2r)}=1-\lambda^{2+r-s(1+r)} \tag{A.17}$$

and rearranging:

$$\lambda^{1+r(1-s)}-\lambda^{2+(2r+1)(1-s)}+\lambda^{1+(1-s)(1+r)}-1=0 \tag{A.18}$$

Thus,

$$\lambda^2(\lambda^{1-s})^{2r+1}-\lambda(\lambda^{1-s})^{1+r}-\lambda(\lambda^{1-s})^r+1=0 \tag{A.19}$$

Introducing a new variable, $y=\lambda^{1-s}$: $1-s=\log_\lambda y$, $s=1-\log_\lambda y$, Eq. (A.19) becomes:

$$\lambda^2 y^{2r+1}-\lambda y^{1+r}-\lambda y^r+1=0 \tag{A.20}$$

In the single-phase spectral cascade model, $r=\frac{1}{2}$, thus:

$$\lambda^2 y^2-\lambda y^{3/2}-\lambda y^{1/2}+1=0 \tag{A.21}$$

This equation has 2 real and 2 complex roots. The real roots are:

$$y_1=\lambda^{-2/3},\quad y_2=\lambda^{-2} \tag{A.22}$$

This corresponds to two negative slopes:

$$s_1=1-\log_\lambda(\lambda^{-2/3})=1-\left(-\frac{2}{3}\right)=\frac{5}{3},$$
$$s_2=1-\log_\lambda(\lambda^{-2})=1-(-2)=3 \tag{A.23}$$

Thus we have shown that the slope which is normally measured in the inertial subrange of turbulent single-phase flows, −5/3, is consistent with the functional form of the transfer terms in Eq. (13) and that it is independent of wave number mesh spacing (λ). Nevertheless, as noted in the text, issues associated with the proper slope are complicated and deserve further study.

References

Bohr, T., Jensen, M.H., Paladin, G., Vulpiani, A., 1998. Dynamical Systems Approach to Turbulence. Cambridge University Press, Cambridge.

Bunner, B., Tryggvason, G., 2003. Effect of bubble deformation on the properties of bubbly flows. J. Fluid Mech. 495, 77–118.

Chaouat, B., Schiestel, R., 2005. A new partially integrated transport model for subgrid-scale stresses and dissipation rate for turbulent developing flows. Phys. Fluids 17, 065106.

Comte-Bellot, G., Corrsin, S., 1966. The use of a contraction to improve the isotropy of grid-generated turbulence. J. Fluid Mech. 25, 657–682.

Desnyanski, V.N., Novikov, E.A., 1974. Simulation of cascade process in turbulent flows. J. Appl. Math. Mech. 38, 468.

Domaradzki, J.A., Rogallo, R.S., 1990. Local energy transfer and nonlocal interactions in homogeneous, isotropic turbulence. Phys. Fluids A 2, 413–426.

Domaradzki, J.A., Liu, W., Hartel, C., Kleiser, L., 1994. Energy transfer in numerically simulated wall-bounded turbulent flows. Phys. Fluids 6, 1583–1599.

Drew, D.A., Passman, S.L., 1998. Theory of Multicomponent Fluids. Springer, Berlin.

Gledzer, E.B., 1973. System of hydrodynamic type allowing 2 quadratic integrals of motion. Sov. Phys. Dokl. 18, 216.

Hinze, J.O., 1975. Turbulence. McGraw-Hill, New York.

Ilic, M., Worner, M., Cacuci, D.G., 2007. Evaluation of energy spectra in bubble driven liquid flows from direct numerical simulations. In: Proceedings of the International Conference on Multiphase Flows, 2007.

Ishii, M., Hibiki, T., 2006.Thermo-Fluid Dynamics of Two-Phase Flow. Springer, Berlin.

Jairazbhoy, V., Tavlarides, L.L., 1995b. A cascade model for neutrally buoyant dispersed two-phase homogeneous turbulence – II. Numerical solution and results. Int. J. Multiphase Flow 21, 485–500.

Jairazbhoy, V., Tavlarides, L.L.Lewalle, J., 1995a. A cascade model for neutrally buoyant dispersed two-phase homogeneous turbulence – I. Model formulation. Int. J. Multiphase Flow 21, 467–483.

Jones, W., Launder, B., 1972. The prediction of laminarization with a two-equation model of turbulence. Int. J. Heat Mass Transfer 15, 301.

Kang, H.S., Chester, S., Meneveau, C., 2003. Decaying turbulence in an active-grid-generated flow and comparisons with large-eddy simulation. J. Fluid Mech. 480, 129–160.

Lahey Jr., R.T., 2005. The simulation of multidimensional multiphase flows. Nucl. Eng. Design 235, 1043–1060.

Lance, M., 1979. Contribution a l'etude de la turbulence dans la phase liquide des ecoulements a bulles, Ph.D. Thesis, L'Universite Claude Bernard de Lyon, France.

Lance, M., Bataille, J., 1991. Turbulence in the liquid phase of a uniform bubbly air/water flow. J. Fluid Mech. 222, 95–118.

Lewalle, J., Tavlarides, L., 1994. A cascade-transport model for turbulent shear flows. Phys. Fluids 6, 3109–3115.

Lopez de Bertodano, M., 1992. Turbulent bubbly two-phase flow in a triangular duct, Ph.D. Thesis, Nuclear Engineering, Rensselaer Polytechnic Institute.

Lumley, J.L., 1978. Computational modeling of turbulent flows. Adv. Appl. Mech. 18, 123.

Nigmatulin, R.I., 1979. Spatial averaging in the mechanics of heterogeneous and dispersed systems. Int. J. Multiphase Flow 5, 353–385.

Ohkitani, K., Yamada, M., 1989. Temporal intermittency in the energy cascade process and local Lyapunov analysis in fully-developed turbulence. Prog. Theor. Phys. 81, 329–341.

Pope, S., 2000. Turbulent Flows. Cambridge University Press, Cambridge.

Rensen, J., Luther, S., Lohse, D., 2005. The effect of bubbles on developed turbulence. J. Fluid Mech. 538, 153–187.

Ruggles, A., Lahey Jr., R.T., Drew, D.A., Scarton, H.A., 1988. An investigation of the propagation of pressure perturbations in bubbly air water flows. J. Heat Transfer 110, 494–499.

Schiestel, R., 1987. Multiple time scales modeling of turbulent flows in one point closures. Phys. Fluids 30, 722.

Veldhuis, C.H.J., Biesheuvel, A., van Wijngaarden, L., Lohse, D., 2005. Motion and wake structure of spherical particles. Nonlinearity 18, C1–C8.

Wilcox, C., 2002. Turbulence Modeling for CFD. DCW Industries, La Canada, CA.